Materials Advances

PAPER

Check for updates

A highly sensitive, selective and room temperature operatable formaldehyde gas sensor using chemiresistive g-C₃N₄/ZnO†

S. P. Subin David, [ID] [a] S. Veeralakshmi, [ID] [a] S. Nehru [ID] *[b] and S. Kalaiselvam [ID] *[a]

Formaldehyde is a common indoor air pollutant whose level has to be monitored by an economic and efficient technique. Here, we report a room temperature operatable g-C₃N₄/ZnO-based formaldehyde gas sensor, showing higher relative sensor response (95.9%) as well as faster response/recovery time (30 s/70 s) at 50 ppm with good linearity, repeatability, selectivity and stability. Further, g-C₃N₄/ZnO shows that the superior performance of HCHO gas sensing compared to both pure g-C₃N₄ and ZnO may be due to the creation of n-n heterojunctions, which achieved the Fermi level equalization and cooperative enhancement of pure components. Thus, the optimization of structure and composition of the present g-C₃N₄/ZnO will offer a promising room-temperature operatable formaldehyde gas sensor in near future.

1. Introduction

Formaldehyde (HCHO) is being continuously released into the indoor environment from numerous sources such as pressed-wood furnitures, laminate flooring, paints, some personal care products, and tobacco smoking, thus causing some serious health issues to humans.[1,2] Therefore, it is urgent to develop a simple, low cost, highly sensitive, selective and stable gas sensor for monitoring HCHO levels.[3,4] In this scenario, chemiresistive semiconductor-type gas sensors have progressively played a vital role in detecting HCHO levels in the indoor/outdoor environment.[5,6] The mechanism of resistive gas sensors is based on the change in the resistance of a sensing layer upon adsorption and reaction with the target gas molecules. The sensing layer usually determines the sensitivity and selectivity.[7] Therefore, sensing materials and structures of the sensing layer have to be properly tuned for the critical sensing performance.

Among semiconducting metal oxides (SMOs),[8] ZnO is a promising material for the sensing of formaldehyde gas due to its excellent sensing response, good selectivity, good thermal and chemical stability, easy fabrication, low cost and non-toxicity.[9,10] Furthermore, ZnO is very sensitive to the surface

environment and even small changes in the surface environment significantly affect the properties of the sensing layer and electron motion, which immediately lead to variations in their resistance.[11] However, pure ZnO is not enough for the high sensitive and selective detection of HCHO gas. Hence, there have been several approaches used to enhance the performance of ZnO by metal doping,[12,13] functionalization of noble metal nanoparticles,[14] inclusion of carbon-based nanomaterials,[15] composition with different metal oxides,[16] *etc.*

Graphitic carbon nitride (g-C₃N₄) is an emergent material for fabricating composites by providing a large scaffold for anchoring numerous inorganic and organic materials. Moreover, it has been explored that g-C₃N₄ matrix-loaded SMOs cooperatively enhance the performance of gas sensors due to their n-type semiconducting property, high specific surface area, exceptional charge transport, good catalytic properties, and significant 2D material characteristics. Particularly, this type of SMO-decorated g-C₃N₄ such as Fe₂O₃/g-C₃N₄ and SnO₂/g-C₃N₄ has shown to create local heterojunctions, which in turn lead to superior gas sensor performance.[17,18] Even the enhancement of the gas sensing properties of ZnO through blending with g-C₃N₄ has been reported against methane gas, and there have been no clear studies on ZnO/g-C₃N₄ against volatile organic compounds (VOCs).[19] Similarly, a ZnO/graphene nanocomposite has also displayed higher formaldehyde gas sensing performance compared to pure ZnO in the concentration range of 2–2000 ppm with good selectivity and fast response/recovery time at higher temperature (200 °C).[20,21]

Most of the HCHO sensors are heated to a high temperature (between 100 °C to 400 °C) for the enhancement of performance,

[a] *Department of Applied Science and Technology, Anna University, A.C. Tech. Campus, Chennai, Tamil Nadu, 600025, India*

[b] *Department of Physical Chemistry, University of Madras, Guindy Campus, Chennai, Tamil Nadu, 600025, India. E-mail: kalai@annauniv.edu, nehruchem@gmail.com*

† Electronic supplementary information (ESI) available. See DOI: 10.1039/d0ma00529k

which in turn leads to a change in the microstructure of the sensing nanomaterials and also increases the power consumption.[22,23] Hence, high temperature gas sensors are not convenient for practical applications due to the fact that they do not fulfil the requirements of the market. Thus, the development of room-temperature operatable gas sensors might solve those struggles such as high power consumption, short device lifetime and reduced explosion hazards. Though few reports are available for the room temperature operatable formaldehyde gas sensors,[24,25] they are not enough to the competitive global market in terms of sensitivity and selectivity.

2. Experimental section

2.1. Materials and methods

Melamine, zinc nitrate hexahydrate, hexamine and sodium hydroxide were obtained from SRL, India. All the calibrated gases were obtained from Chemix special gases and equipments, India. All other chemical reagents were of analytical grade and double-distilled water was used throughout the studies. The crystalline structure of the as-prepared composite was characterized via X-ray diffractometry (D2 Phaser, Bruker). UV-visible diffuse reflectance spectra (UV-Vis DRS) of the samples were recorded in the wavelength range of 200–800 nm using a PerkinElmer, Lambda 850 UV/Vis spectrophotometer equipped with an integrating sphere accessory using $BaSO_4$ as the reference. The surface morphology of samples was determined via field emission scanning electron microscopy (FE-SEM) using a JEOL JSM-7610F instrument and transmission electron microscopy (TEM) using a JEOL 2100F instrument.

2.2. Synthesis of g-C₃N₄

Pristine g-C_3N_4 was synthesized on the basis of a previously reported procedure.[26] In brief, 5.0 g of melamine was calcined at 550 °C for 4 h at a heating rate of 3.5 °C min⁻¹ in a muffle furnace. The obtained yellow agglomerate was ground into powder, followed by washing with water and ethanol. Then, the sample was dried at 80 °C for 12 h and stored in a vacuum desiccator.

2.3. Synthesis of ZnO and g-C₃N₄/ZnO

ZnO and g-C_3N_4/ZnO were synthesized by slight modification in the reported procedure.[27] A solution of 0.5 g of hexamine and 0.75 g of zinc nitrate hexahydrate in 90 mL of water was stirred for 30 min. Then, the pH of the solution was adjusted to 11 using a 1 M NaOH solution. The resulting solution was stirred for 1 h and transferred into a Teflon crucible, followed by keeping it inside an autoclave at 140 °C for 2 h. After cooling to room temperature, the obtained product was filtered and washed repeatedly with distilled water and ethanol. The product was dried in a vacuum oven at 60 °C for 24 h. The resulted product was further dried at 160 °C for 12 h to increase the crystallinity.

About 0.25 g of g-C_3N_4 was dispersed in 30 mL of water, followed by ultra-sonication for 30 min. A solution of 0.5 g of hexamine and 0.75 g of zinc nitrate hexahydrate in 90 mL of water was stirred for 30 min. After adding the g-C_3N_4 solution to the above mixture, the pH of the solution was adjusted to 11 using a 1 M NaOH solution. Then, the same above methodology was followed to synthesis g-C_3N_4/ZnO.

2.4. Fabrication and measurement of the gas sensor

About 0.01 g of the sample in 100 μL of water was uniformly dispersed by sonicating for 15 min, and the resulting paste was then coated on the surface of a ceramic plate (length = 9 mm; width = 7 mm; thickness = 2 mm) on which a pair of Ag wire was previously printed using an Ag paste. The sample paste was coated by the doctor blade method on the ceramic substrate, and the active area of device was about 5×5 mm. A custom-made gas sensor setup of 1 liter volume was fabricated, as illustrated in Fig. S5 (ESI†), and the resistivity of the materials was measured using a highly sensitive control unit consisting of a GDM-8261A 61/2 Digital Dual Measurement Multimeter. All the experiments were performed at room temperature (27 ± 1 °C) and maintained the relative humidity to 60 ± 5 RH.

3. Results and discussion

Structural and surface morphological analysis

The XRD pattern for the as-synthesized ZnO, g-C_3N_4 and g-C_3N_4/ZnO are shown in Fig. 1. The XRD pattern of ZnO shows that the peaks at 2θ of $31.7°$, $34.4°$, $36.2°$, $47.5°$, $56.5°$, $62.8°$, $66.3°$,67.9, $69.0°$, $72.6°$ and $76.8°$ correspond to the planes of (100), (002), (101), (102), (110), (103), (200), (201), (112), (004) and (202), in accordance with the hexagonal structure (JCPDS No. 00-036-1451).[27] The XRD pattern of g-C_3N_4 shows a peak at $27.5°$, which corresponds to the interlayer stacking of aromatic segments and tri-s-triazine units of g-C_3N_4 assigned to the (002) plane and the same peak has been also observed in the g-C_3N_4/ZnO composite. The positions and shapes of the characteristic peaks of the g-C_3N_4/ZnO composite are similar to those of pure
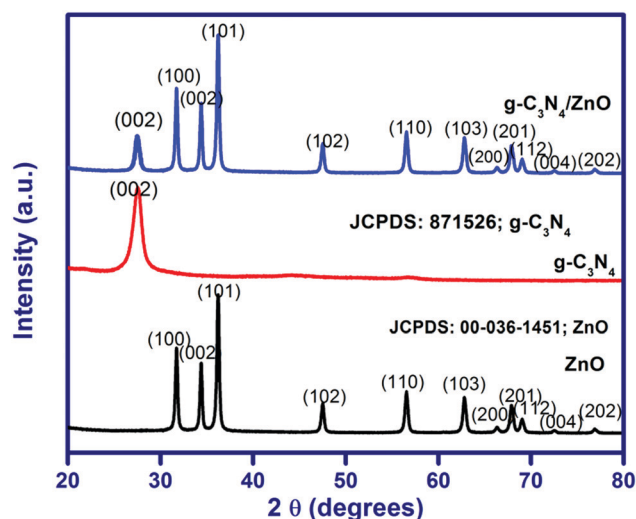

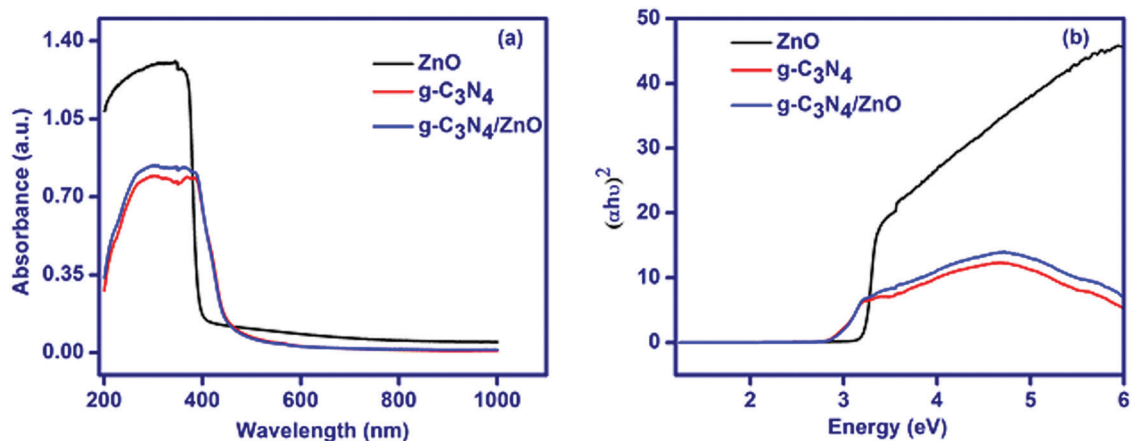Fig. 1 XRD pattern of ZnO, g-C_3N_4 and g-C_3N_4/ZnO.

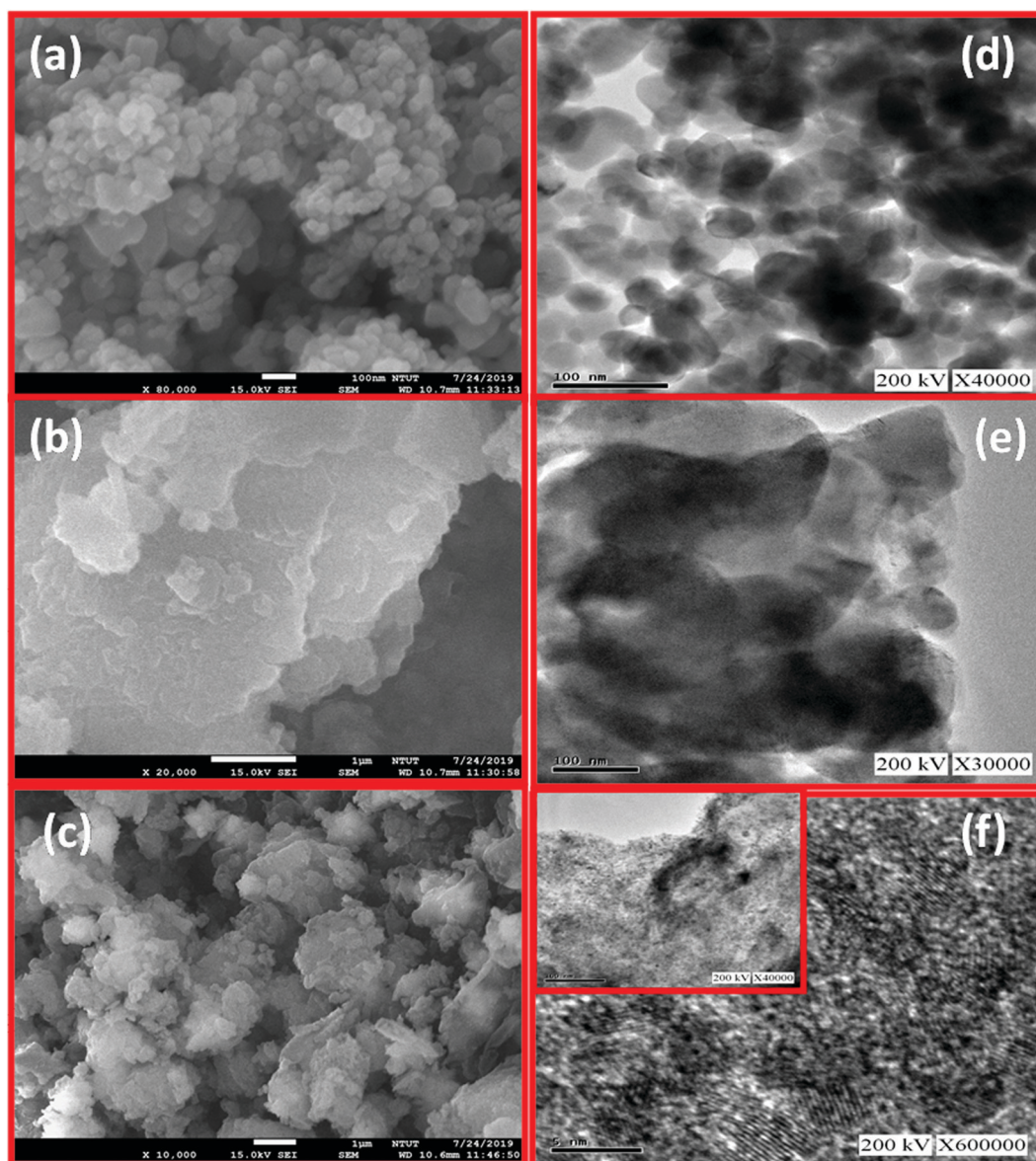**Fig. 2** (a) UV-visible diffuse reflectance spectra and (b) Tauc plot for ZnO, g-C₃N₄ and g-C₃N₄/ZnO.

Fig. 3 FE-SEM images of (a) ZnO (b) g-C₃N₄ (c) g-C₃N₄/ZnO; TEM images of (d) ZnO (e) g-C₃N₄ (f) g-C₃N₄/ZnO.

Paper

ZnO and g-C$_3$N$_4$, and no other new peaks are observed in the obtained XRD pattern.

UV-visible diffuse reflectance spectra of ZnO, g-C$_3$N$_4$ and g-C$_3$N$_4$/ZnO are shown in Fig. 2(a). The band gap energy of ZnO, g-C$_3$N$_4$ and g-C$_3$N$_4$/ZnO could be calculated by the Tauc eqn (1):[28]

$$\alpha h\nu = A(h\nu - E_g)^{n/2} \qquad (1)$$

where α, h, ν, A and E_g are the absorption coefficient of the material, Planck's constant, frequency of light, proportionality constant and band gap energy, respectively. The value of n depends on the transition type of the semiconductor ($n = 4$ for indirect transition and $n = 1$ for direct transition). It is known that ZnO is a material of direct band gap, hence the value of n is equal to 1.[28] From the plot of $(\alpha h\nu)^2$ *vs.* $h\nu$ in the Fig. 2(b), the extrapolation of the linear part of the graph to the *x*-axis results in the E_g values for ZnO, g-C$_3$N$_4$ and g-C$_3$N$_4$/ZnO as 3.21, 2.82, and 2.78 eV, respectively. This decrease in the band gap energy clearly implies that there is an effective formation of tight chemically bonded interfaces between the g-C$_3$N$_4$ and ZnO phases in the g-C$_3$N$_4$/ZnO composite. That is, according to the energy band theory, the composite effect should decrease the gap because of the splitting of each level into n levels equal to the number of interacting atoms. Therefore, the bands may come closer or overlap in case of the nanocomposite sample.[29]

In FE-SEM images of Fig. 3(a and b), ZnO and g-C$_3$N$_4$ appear as regular granules and nanosheets, respectively. After the formation of the g-C$_3$N$_4$/ZnO nanocomposite, the surface morphology becomes aggregated granules along with nanosheets, as shown in Fig. 3(c), indicating the effective mixing of the ZnO and g-C$_3$N$_4$ phases. In the TEM images of Fig. 3(d and e), ZnO and g-C$_3$N$_4$ look like hexagonal particles (43 ± 10 nm) and nanosheets, respectively. Moreover, the TEM images of the g-C$_3$N$_4$/ZnO nanocomposite in Fig. 3(f) show well-dispersed ZnO particles in the matrix of g-C$_3$N$_4$ with well-reduced particle sizes of 9 ± 3 nm with the effective mixing of ZnO and g-C$_3$N$_4$ phases. These reduced sizes of particles with the effective mixing of phases form a heterojunction between the phases, which may be helpful to improve the gas sensing properties.

Gas sensor studies

Preliminarily, gas sensor studies for g-C$_3$N$_4$, ZnO and g-C$_3$N$_4$/ZnO were tested against 50 ppm concentration of nine different gases namely methanol, ethanol, isopropanol, *n*-butanol, formaldehyde, acetone, benzene, toluene and xylene at room temperature and 60% RH (Fig. 4). Based on the changes in the chemiresistive properties of g-C$_3$N$_4$, ZnO and g-C$_3$N$_4$/ZnO in the absence and presence of nine different gases, the following parameters have been calculated using the eqn (2) and (3).[15]

$$\text{Sensor response (in times)} = R_a/R_g \qquad (2)$$

$$\text{Sensor response (\%)} = (R_a - R_g)/R_a \times 100 \qquad (3)$$

where R_a and R_g are the resistances of the sensor in air and test gas, respectively. Sensitivity is the slope of the calibration curve,
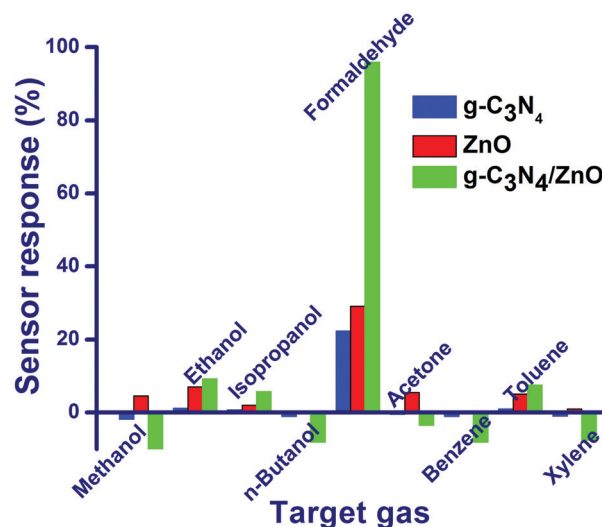

Fig. 4 Relative gas sensor response (%) of g-C$_3$N$_4$, ZnO and g-C$_3$N$_4$/ZnO against 50 ppm concentration of nine different gases such as methanol, ethanol, isopropanol, *n*-butanol, formaldehyde, acetone, benzene, toluene and xylene at room temperature at 60% RH.

that is, sensor response *versus* target gas concentration, as given in eqn (4),[7]

$$\text{Sensitivity} = \text{Response (in times)/Concentration} \\ \text{(in ppm)} \qquad (4)$$

By following the change in the chemiresistance of the sensor between air and exposed gas, a relative sensor response was plotted against different gases using eqn (2) and it can be clearly seen from Fig. 4 that g-C$_3$N$_4$-, ZnO- and g-C$_3$N$_4$/ZnO-based sensors more selectively detect the HCHO gas compared to other gases.

Particularly, g-C$_3$N$_4$ and ZnO show moderate relative sensor response values of 22.4% and 29.1%, respectively, against HCHO. However, g-C$_3$N$_4$/ZnO shows the highest relative sensor response (95.9%) towards formaldehyde compares to other gases may be due to the cooperative effect of g-C$_3$N$_4$, and ZnO in the sensing mechanism. To the best of our search, the present g-C$_3$N$_4$/ZnO-based sensor displays the highest sensor response value at room temperature for the detection of formaldehyde (Table 1).

Hence, gas sensor studies for g-C$_3$N$_4$, ZnO and g-C$_3$N$_4$/ZnO were elaborated against HCHO gas in the concentration range of 1–1000 ppm by monitoring change in the resistance by alternative exposure of air and HCHO gas (Fig. 5a and Fig. S1(a), (b), ESI†). As shown in Fig. 5a, the resistance of g-C$_3$N$_4$/ZnO is stable in air, and the value gets reduced suddenly upon the exposure of HCHO gas and then reaches a steady value. Upon expelling the HCHO gas from the chamber, the original resistance value of the sensor is again reverted for all concentrations studied. Further, the g-C$_3$N$_4$/ZnO-based sensor also has significant reversibility in the detection of the formaldehyde gas on a rapid switching between air and gas.

Sensor responses for g-C$_3$N$_4$, ZnO and g-C$_3$N$_4$/ZnO were calculated using eqn (3), and they are plotted against time for the all concentrations studied (Fig. 5b and Fig. S2(a), (b), ESI†).

Table 1 Comparison of the formaldehyde gas sensing performance in the previously published works

S. No.	Sensing material	Conc. in ppm	Operating temperature (°C)	Response	Response/Recovery time (s)	Ref.
1	ZnO	5	RT	[a]1.91	332/736	30
2	Au@ZnO	5	RT	[a]10.57	138/104	30
3	Zn_2SnO_4	50	230	[a]23.57	15/17	31
4	rGO/ZnO	45	RT	[b]8	—	32
5	$rGO/ZnWO_3$	10	95	[a]21.4	—	33
6	$rGO/ZnSnO_3$	10	103	[a]12.8	—	34
7	Ag/ZnO	300	100	[b]7.5	20/4	23
8	MnO_2/ZnO	320	100	[b]17	27/12	35
9	Li/ZnO	350	100	[b]40.2	8/26	31
10	NiO/ZnO	200	100	[b]26.2	18/30	36
11	Fe doped ZnO	10	300	[a]33	—	30
12	ZnO doped In_2O_3	100	260	[a]9	—	32
13	ZnO/Co_3O_4 hollow sphere	10	160	[a]5.8	27/15	37
14	Graphene/ZnO nanosheets	100	200	[a]12	10/29	38
15	rGO/flower like ZnO	10	RT	[a]6.5	—	25
16	$rGO/ZnSnO_3$ microshperes	10	103	[a]12.8	87/31	34
17	Fe–ZnO/rGO	5	120	[a]12.7	34/37	1
18	ZnO	50	RT	[b]29.1	180/30	Present work
19	$g-C_3N_4$	50	RT	[b]22.4	690/50	Present work
20	$g-C_3N_4/ZnO$	50	RT	[b]95.9	30/70	Present work

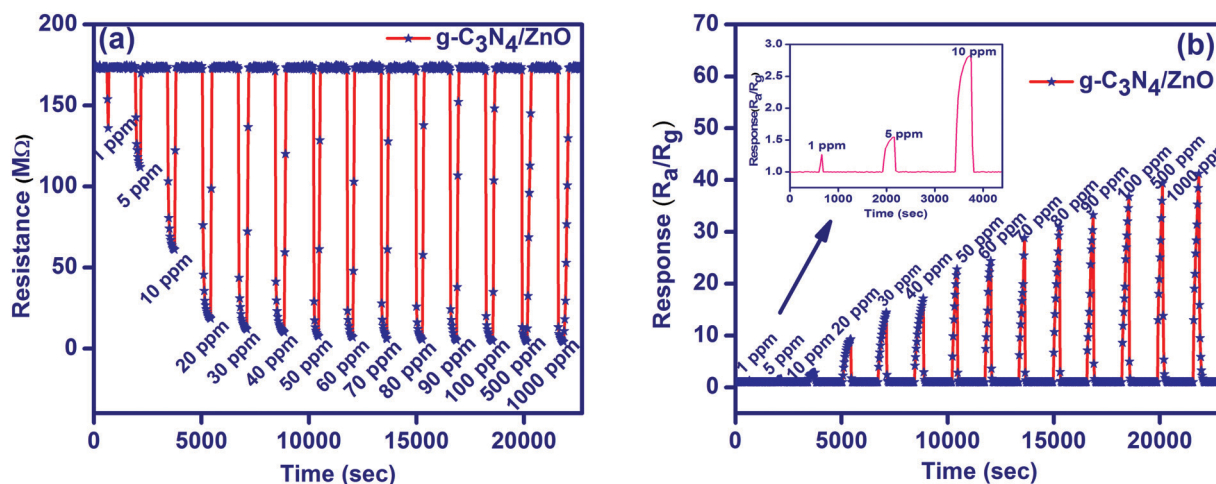RT – Room temperature. [a] Response (%) = $(R_g - R_a)/R_a$. [b] Response = R_a/R_g.

Fig. 5 (a) Resistance plot and (b) response plots for the sensing of formaldehyde gas at room temperature.

$g-C_3N_4/ZnO$ shows a linear increase in the sensor response (about 1.3 to 41 times) with respect to the increase in the HCHO concentration (1–1000 ppm). However, only moderate sensor responses were observed for both $g-C_3N_4$ (about 1.0 to 3 times) and ZnO (about 1.1 to 2.2 times).

The gas sensor performances such as sensitivity and response speed are dependent on the rates of diffusion of a target gas and its surface reaction. The gas diffusion rate is limited by the microstructure of the sensing layer and the size of the target gas molecules, while the surface reaction rate is dependent on the catalytic activity of the sensing layer and operating temperature. Importantly, the rate leading to the steady state, where the diffusion and surface reaction are balanced, determines the response speed of gas sensors. Therefore, the gas diffusion and surface reaction are crucial parameters for semiconductor gas sensors. As shown in Fig. 6a,

for the 50 ppm of HCHO, response/recovery properties for $g-C_3N_4/ZnO$ (30 s/70 s) is good compared to pure $g-C_3N_4$ (690 s/50 s) and ZnO (180 s/30 s). The observed lower response for the $g-C_3N_4/ZnO$ composite indicates that the gas sensor readily gains the electron by the adsorption reaction of HCHO molecules. However, the $g-C_3N_4/ZnO$ composite has relatively a higher recovery time to go back to the original state in the presence of air due to the decrease in the surface electron density. Further, the sensitivities of $g-C_3N_4$, ZnO and $g-C_3N_4/ZnO$ were also compared by plotting the sensor response versus concentration of formaldehyde for the tested concentration range (Fig. 6(b) and Fig. S3, ESI†). The obtained plots illustrate the good linearity of the gas sensor, which is required for the quantitative detection of formaldehyde gas. In addition, $g-C_3N_4/ZnO$ showed a high sensitivity value (0.372 ppm^{-1}) compared to both $g-C_3N_4$ (0.005 ppm^{-1}) and ZnO (0.020 ppm^{-1}).
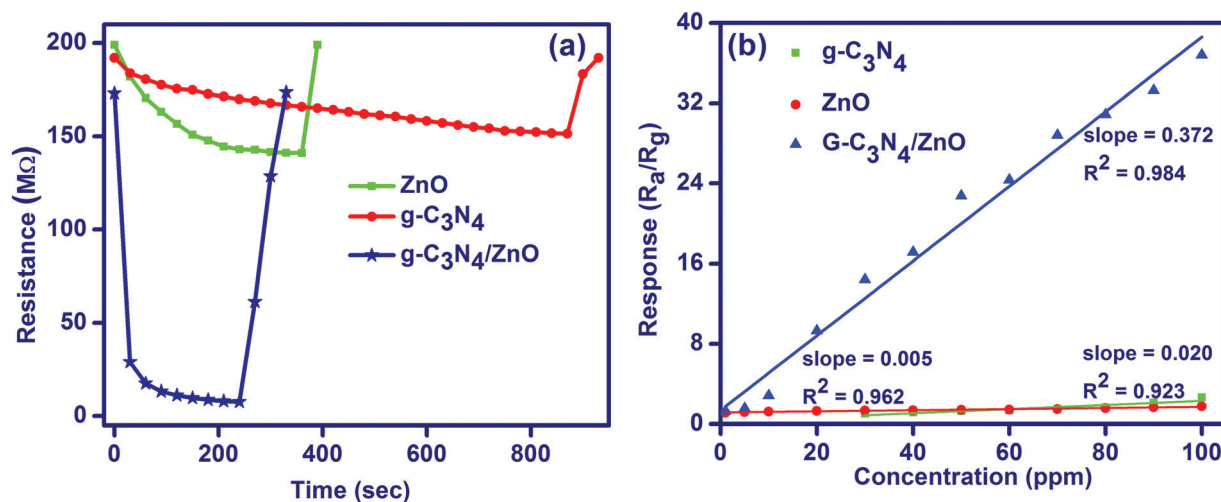
Fig. 6 (a) Response–recovery plot and (b) sensitivity plot for the sensing of formaldehyde gas at room temperature.

The performance of the g-C_3N_4/ZnO sensor against 50 ppm of formaldehyde gas was also analyzed by checking (i) the repeatability of the sensor response for the five repeated response/recovery cycles (Fig. 7(a)), (ii) long term reproducibility of the sensor response for 52 days (Fig. 7(b)), and (iii) dynamic stability of the measured resistance value before and after the
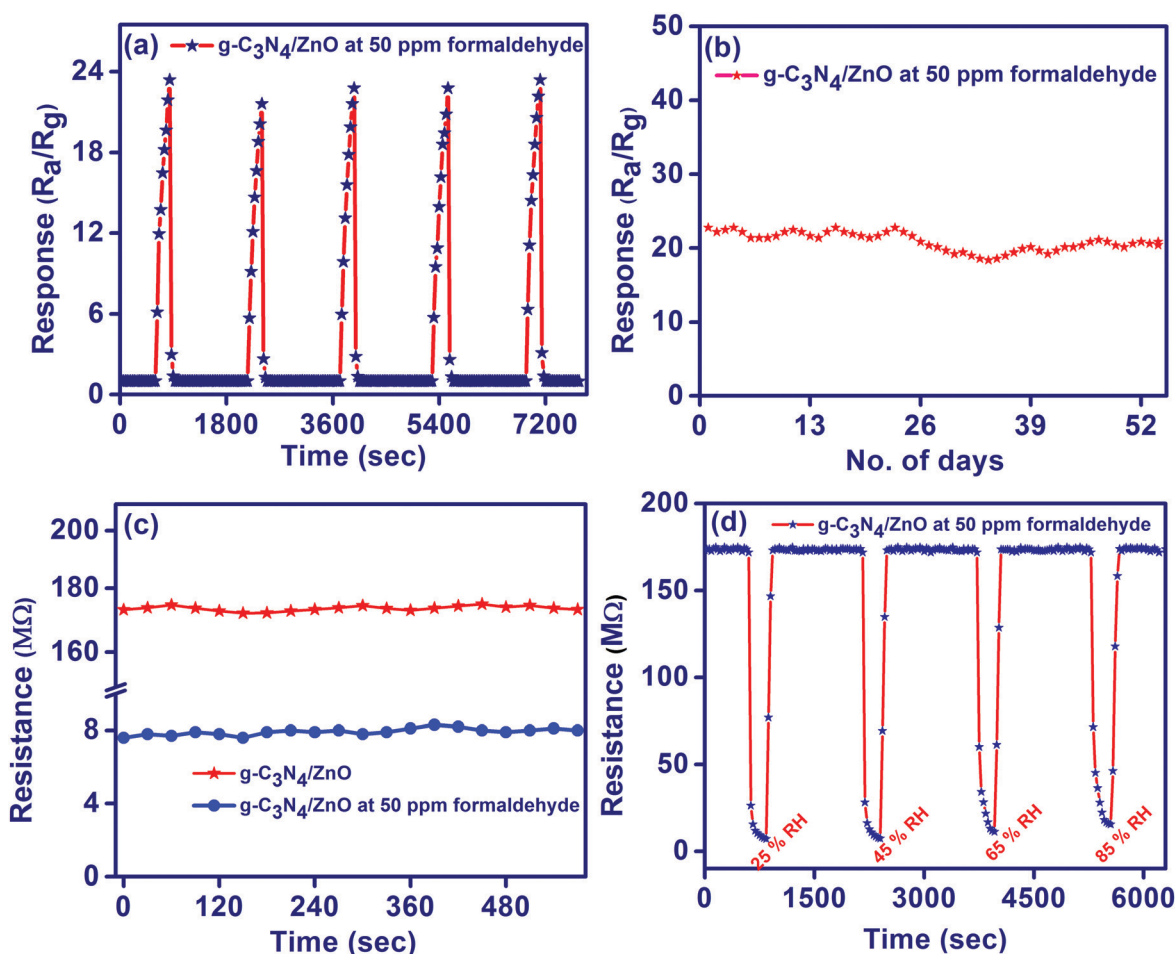

Fig. 7 (a) Repeatability of the sensor response for the five successive cycles against 50 ppm of HCHO gas (b) long term reproducibility of the HCHO gas sensor response at 50 ppm (c) Stability of the measured resistance value before and after the exposure of 50 ppm of HCHO gas and (d) resistance plot at different humidity levels, for g-C_3N_4/ZnO.

exposure of gas for 30 min (Fig. 7(c)). The obtained results evidence the excellent stability and reproducibility of the g-C_3N_4/ZnO-based gas sensor for the detection of formaldehyde gas. Further, the effect of relative humidity on the performance of the g-C_3N_4/ZnO-based gas sensor was investigated by exposing the sensor at 50 ppm of formaldehyde gas under numerous relative humidity conditions (25% RH, 45% RH, 65% RH and 85% RH). As shown in Fig. 7(d), the resistance of g-C_3N_4/ZnO at 50 ppm of formaldehyde gas under 25%, 45%, 65% and 85% RH reached 7.22, 7.45, 7.60 and 8.56 MΩ, respectively. That is, the sensor response is slightly decreased to 23.96, 23.23, 22.76 and 20.22 with the increase in the respective RH value of 25–85% RH, as shown in Fig. S4(b) (ESI†), may be due to the minor interference of water molecules with the surface adsorbed oxygen species of the gas sensor.[39]

Further, it is also noted in Fig. S4(b) (ESI†) that the sensor response (ratio of the sensor resistance under air (R_a) to the sensor resistance under a relative humidity (R_{RH})) of g-C_3N_4/ZnO slightly increases to the values of 1.03, 1.07, 1.14 and 1.47 upon respective increase in the relative humidity from 25 to 85% RH due to a decrease in the R_{RH} value by favouring the charge transfer from water molecules to the nanostructures under a higher relative humid environment. Thus, the resistance and response of the proposed g-C_3N_4/ZnO sensor is almost unchanged when the RH value is below 60%, *i.e.*, it has a capability of anti-interference towards water vapour.[7]

The HCHO gas sensing mechanism of present materials can be explained based on the phenomenon of gas adsorption-induced charge transfer (Fig. 8). Upon exposing the gas sensor to air, oxygen molecules get adsorbed on the surface of the gas sensor and are converted into chemisorbed oxygen species (O_2^-, O^- and O^{2-}) by gaining electrons from the conduction band of the gas sensor. Thus electron density in the sensing layer of gas sensor gets diminished, which leads to the formation of a larger depletion layer. The majority charge carriers in an n-type semiconductor such as g-C_3N_4 and ZnO are electrons. Upon exposing the gas sensor to reducing (electron donating) gases such as HCHO, chemisorbed oxygen species react with HCHO and release the electrons back into the depletion layer of the gas sensor. Thus, the resistivity of the gas sensor gets decreased.[40]

The observed superior HCHO gas sensing performance of g-C_3N_4/ZnO can be attributed by the formation of potential active sites in the g-C_3N_4/ZnO sensor as compared with the both g-C_3N_4 and ZnO sensors *via* the creation of an n–n heterojunction between n-type g-C_3N_4 and n-type ZnO.[19] Further, the sensing performance can be also favoured by achieving the Fermi level equalization through a flow of electrons from a higher Fermi level of g-C_3N_4 to a lower Fermi level of ZnO at the interface of g-C_3N_4 and ZnO. Hence, upon the exposure of the HCHO gas on the g-C_3N_4/ZnO sensor, chemisorbed oxygen anions may release trapped electrons back to ZnO and additional electrons may enter into ZnO from g-C_3N_4 through the n–n heterojunction, leading to the cooperative enhancement of HCHO gas detection.[41] Further, it is also reported that metal oxides such ZnO catalytically oxidize HCHO. In addition, g-C_3N_4 in the air atmosphere can also promote oxygen molecules to form functional groups, such as hydroxyl (*OH), which can facilitate the oxidation of HCHO molecules.[42]

4. Conclusion

In summary, the g-C_3N_4/ZnO nanocomposite selectively detected formaldehyde gas as compared to other volatile organic gases such as methanol, ethanol, isopropanol, *n*-butanol, acetone, benzene, toluene and xylene at room temperature. Formaldehyde gets sensed at the highest relative sensor response value of 95.9%, which is approximately three times higher than that of both g-C_3N_4 and ZnO. Further, the sensor response of g-C_3N_4/ZnO against formaldehyde gas was almost unchanged when RH value is below 65%. For the first time in literature, we reported a room temperature operatable g-C_3N_4/ZnO-based formaldehyde gas sensor with lower concentration detection, quick response, good repeatability and excellent stability. However, a detailed investigation is needed for the clear understanding of the gas sensing mechanism as well as contribution of g-C_3N_4 and ZnO in the cooperative effect, which are still in the pipeline. By optimising the composition of g-C_3N_4/ZnO, it is very much possible to develop a room temperature operatable and real time monitorable formaldehyde gas sensor in near future.

Fig. 8 Mechanism of the gas sensing process.

Conflicts of interest

There are no conflicts to declare.

References

1 W. Guo, B. Zhao, Q. Zhou, Y. He, Z. Wang and N. Radacsi, *ACS Omega*, 2019, **4**, 10252–10262.

2 A. Mirzaei, J.-H. Kim, H. W. Kim and S. S. Kim, *J. Mater. Chem. C*, 2018, **6**, 4342–4370.

3 H. Long, A. Harley-Trochimczyk, S. Cheng, H. Hu, W. S. Chi, A. Rao, C. Carraro, T. Shi, Z. Tang and R. Maboudian, *ACS Appl. Mater. Interfaces*, 2016, **8**, 31764–31771.

4 E.-X. Chen, H.-R. Fu, R. Lin, Y.-X. Tan and J. Zhang, *ACS Appl. Mater. Interfaces*, 2014, **6**, 22871–22875.

5 J. Zhang, Z. Qin, D. Zeng and C. Xie, *Phys. Chem. Chem. Phys.*, 2017, **19**, 6313–6329.

6 H. Yu, T. Yang, R. Zhao, B. Xiao, Z. Li and M. Zhang, *RSC Adv.*, 2015, **5**, 104574–104581.

7 S. S. David, S. Veeralakshmi, J. Sandhya, S. Nehru and S. Kalaiselvam, *Sens. Actuators, B*, 2020, 128410.

8 C. Wang, X. Cheng, X. Zhou, P. Sun, X. Hu, K. Shimanoe, G. Lu and N. Yamazoe, *ACS Appl. Mater. Interfaces*, 2014, **6**, 12031–12037.

9 Q. Huang, D. Zeng, H. Li and C. Xie, *Nanoscale*, 2012, **4**, 5651–5658.

10 H. Tian, H. Fan, M. Li and L. Ma, *ACS Sens.*, 2016, **1**, 243–250.

11 X. Li, C. Wang, X. Zhou, J. Liu, P. Sun and G. Lu, *RSC Adv.*, 2014, **4**, 47319–47324.

12 M. H. Darvishnejad, A. A. Firooz, J. Beheshtian and A. A. Khodadadi, *RSC Adv.*, 2016, **6**, 7838–7845.

13 Z. Wang, C. Hou, Q. De, F. Gu and D. Han, *ACS Sens.*, 2018, **3**, 468–475.

14 P. Rai, S. M. Majhi, Y.-T. Yu and J.-H. Lee, *RSC Adv.*, 2015, **5**, 76229–76248.

15 A. Bag and N.-E. Lee, *J. Mater. Chem. C*, 2019, **7**, 13367–13383.

16 C. Wang, L. Yin, L. Zhang, D. Xiang and R. Gao, *Sensors*, 2010, **10**, 2088–2106.

17 Y. Xu, S. Huang, M. Xie, Y. Li, H. Xu, L. Huang, Q. Zhang and H. Li, *RSC Adv.*, 2015, **5**, 95727–95735.

18 J. Cao, C. Qin, Y. Wang, H. Zhang, B. Zhang, Y. Gong, X. Wang, G. Sun, H. Bala and Z. Zhang, *RSC Adv.*, 2017, **7**, 25504–25511.

19 X. Li, Y. Li, G. Sun, N. Luo, B. Zhang and Z. Zhang, *Nanomaterials*, 2019, **9**, 724.

20 V. Galstyan, E. Comini, I. Kholmanov, G. Faglia and G. Sberveglieri, *RSC Adv.*, 2016, **6**, 34225–34232.

21 F. Meng, Y. Chang, W. Qin, Z. Yuan, J. Zhao, J. Zhang, E. Han, S. Wang, M. Yang and Y. Shen, *ACS Appl. Nano Mater.*, 2019, **2**, 2734–2742.

22 Y. Tie, S. Ma, S. Pei, K. Zhu, Q. Zhang, R. Zhang, B. Wang, J. Zhang, X. Xu and T. Han, *Mater. Lett.*, 2020, **259**, 126896.

23 G. Zhu, Y. Liu, H. Xu, Y. Chen, X. Shen and Z. Xu, *CrystEngComm*, 2012, **14**, 719–725.

24 F.-C. Chung, Z. Zhu, P.-Y. Luo, R.-J. Wu and W. Li, *Sens. Actuators, B*, 2014, **199**, 314–319.

25 X. Li, J. Wang, D. Xie, J. Xu, R. Dai, L. Xiang, H. Zhu and Y. Jiang, *Sens. Actuators, B*, 2015, **221**, 1290–1298.

26 J. Meng, J. Pei, Z. He, S. Wu, Q. Lin, X. Wei, J. Li and Z. Zhang, *RSC Adv.*, 2017, **7**, 24097–24104.

27 S. P. Adhikari, H. R. Pant, H. J. Kim, C. H. Park and C. S. Kim, *Ceram. Int.*, 2015, **41**, 12923–12929.

28 N. Kamarulzaman, M. F. Kasim and R. Rusdi, *Nanoscale Res. Lett.*, 2015, **10**, 346.

29 N. Kumaresan, M. M. A. Sinthiya, M. P. Kumar, S. Ravichandran, R. R. Babu, K. Sethurman and K. Ramamurthi, *Arabian J. Chem.*, 2020, **13**, 2826–2843.

30 W. Guo, *J. Electrochem. Soc.*, 2016, **163**, B517.

31 J. Zhao, C. Xie, L. Yang, S. Zhang, G. Zhang and Z. Cai, *Appl. Surf. Sci.*, 2015, **330**, 126–133.

32 H. Yang, S. Wang and Y. Yang, *CrystEngComm*, 2012, **14**, 1135–1142.

33 M. A. Ashraf, Z. Liu, W. Peng and Z. Parsaee, *Anal. Chim. Acta*, 2019, **1051**, 120–128.

34 J. Sun, S. Bai, Y. Tian, Y. Zhao, N. Han, R. Luo, D. Li and A. Chen, *Sens. Actuators, B*, 2018, **257**, 29–36.

35 C. Xie, L. Xiao, M. Hu, Z. Bai, X. Xia and D. Zeng, *Sens. Actuators, B*, 2010, **145**, 457–463.

36 X. San, M. Li, D. Liu, G. Wang, Y. Shen, D. Meng and F. Meng, *J. Alloys Compd.*, 2018, **739**, 260–269.

37 S. Bai, J. Guo, X. Shu, X. Xiang, R. Luo, D. Li, A. Chen and C. C. Liu, *Sens. Actuators, B*, 2017, **245**, 359–368.

38 Z.-W. Chen, Y.-Y. Hong, Z.-D. Lin, L.-M. Liu and X.-W. Zhang, *Electron. Mater. Lett.*, 2017, **13**, 270–276.

39 Y. Xu, L. Zheng, C. Yang, W. Zheng, X. Liu and J. Zhang, *Sens. Actuators, B*, 2020, **310**, 127846.

40 N. Li, Y. Fan, Y. Shi, Q. Xiang, X. Wang and J. Xu, *Sens. Actuators, B*, 2019, **294**, 106–115.

41 W.-K. Jo and N. C. S. Selvam, *J. Hazard. Mater.*, 2015, **299**, 462–470.

42 Y. Jiao, Y. Zheng, M. Jaroniec and S. Z. Qiao, *J. Am. Chem. Soc.*, 2014, **136**, 4394–4403.